ISSN/1120-5598

ENTE PER LE NUOVE TECNOLOGIE
L'ENERGIA E L'AMBIENTE

Associazione EURATOM-ENEA sulla Fusione

Contributions to the SIXth INTERNATIONAL CONFERENCE ON FUSION REACTOR MATERIALS

(Stresa, Italy, 27 September 1 October 1993)

ENEA - Dipartimento Energia, Fusione
Centro Ricerche Energia Frascati

RT/ERG/FUS/93/17

Manuscript received in final form on July 1992

Printed on November 1993

This report has been prepared, printed and distributed by: *Servizio Studi e Documentazione* - ENEA, Centro Ricerche Energia Frascati, C.P. 65 - 00044 Frascati, Rome, Italy.

Published by ENEA, Direzione Centrale Relazioni, Viale Regina Margherita 125, Rome, Italy

CONTENTS

OUTGASSING TESTS ON GRAPHITES IN THE TEMPERATURE RANGE 373÷1873 K

C. Alessandrini, M.L. Apicella, L. Verdini

Associazione EURATOM-ENEA sulla Fusione, C.R.E. Frascati,
P.O. Box 65 - 00044 Frascati, (Rome) (Italy)

ABSTRACT

Graphite is a an interesting material for plasma-facing components in fusion experiments, mainly because of its low atomic number and its excellent thermal properties. Nevertheless, it contains a large amount of gaseous impurities, which can be released by plasma-surface interaction and affect the purity of the deuterium-tritium plasma. To investigate the outgassing behaviour of graphites, CFCs and doped C composites, a facility has been set up to perform outgassing tests on samples (dim. 0.02x0.02x0.005 m), as a function of temperature in the range between 373 and 1873 K. The experimental apparatus, designed to work in UHV conditions, allows outgassing measurements by a quadrupole mass spectrometer (1-200 AMU), using two different methods. The test facility, the quadrupole calibration and quantitative outgassing measurements on SEP CARB N112 and DUNLOP V graphites are described.

1. Introduction

In the framework of the European Fusion Technology Programme, the Fusion Technology Division of ENEA has been assigned with the task of performing outgassing tests on candidate materials for the NET plasma-facing components.

In detail, the work consists in evaluating the outgassing behaviour of samples made of graphites, CFCs and doped C composites, by measuring the outgassing rate of H_2, H_2O, O_2, CO, CO_2 and CxHy species, as a function of temperature in the range 373-1873 K and of pre-treatments.

An ad hoc facility has been built to measure the outgassing rate of samples (dim. 0.02x0.02x0.005 m)). The measuring apparatus, designed to work in UHV conditions, allows outgassing measurements by means of a quadrupole mass spectrometer (1-200 AMU) in two different ways:

a) pressure rise method;

b) known conductance method.

In the first method, the outgassing rate is measured by recording the increase of the total and partial pressures immediately after exclusion of the pumping system.

In the second, the measuring chamber is dynamically pumped through a known conductance.

The outgassing rate is calculated by measuring the total and partial pressures and taking into account the effective pumping speed for each gas in the chamber.

The sample is heated up to 1873 K, using a RF inductive system. This technique was chosen to avoid heating other components in the vacuum chamber. To keep the outgassing noise level of the measuring chamber low and constant, the samples are inserted under vacuum by a load lock device.

2. Description of the test facility

The test facility (see Fig. 1) consists of a stainless steel measuring chamber, 0.3 m in diameter, and 0.4 m high, capable of reaching a base pressure in the range of 10^{-7} Pa, since it is pumped by a 0.5 m^3/s turbomolecular pump.

The measuring chamber is connected to the turbo through two vacuum lines, each with its gate valve, one (0.15 m diam.) serving as the main pumping connection, the other (0.1 m diam.) with the insertion of a 0.01-m-diam. diaphragm used as by-pass for known conductance measurements. The sample is supported in the measuring chamber by a fork consisting of two parallel 1.5×10^{-3} m-diam. tungsten wires inserted in two holes made in the sample.

Due to the reactions expected between graphite and refractory metals at high temperatures and in order to enable the extraction of the sample from its support, the contact between the sample and the tungsten wires is not direct but via intermediate tantalum tubes placed in the holes of the sample.

The facility is provided with a load lock chamber and a transfer system for inserting or extracting the sample under vacuum. The load lock chamber, connected to the measuring chamber through a 100 CF gate valve, consists of a 100 CF, six-way commercial cross pumped by a 0.11 m^3/s turbomelecular pump.

The transfer system consists of pliers shaped to accomodate the sample, which can be grasped or released thanks to two cams driven by a rotary feedthrough. The pliers are mounted on one end of a rod, which is able to move (0.45 m stroke) from the load lock chamber to the measuring chamber by means of a rack and pignon device driven by a second rotary feedthrough. All the moving parts of the system are metallic and are lubricant-free since they are supported by ball bearings. The device allows highly precise and reproducible positioning of the sample (errors within 1×10^{-4} m). The inductive method was chosen to a heat the sample with a 22 kW, 500 KHz power supply providing 12 kW of RF power at the coil.

The coil consists of four turns of 5×10^{-3} m-diam., 1×10^{-3} m-thick copper tubing with an internal coil diameter of 3×10^{-2} m. The coil is water cooled and connected to two electrical feedthroughs sealed on an alumina disc by means of viton "o" rings. Their utilization was inevitable, since any of the commercial ceramic-metal feedthroughs welded on a metallic flange would give rise to the RF heating effect of the metal between the two conductors.

The sample temperature is measured from 373 K to 1873 K through two sapphire windows, by two infrared pyrometers. To cover the whole temperature range, it was necessary to install two different pyrometers, one for 373 to 823 K, the other for 773 to 1873 K. The pyrometers are connected to the temperature control system, which automatically switches from one pyrometer to the other when the first approaches to its full scale and vice versa.

The programmable temperature control system connected to the RF power supply provides feedback control of the temperature and allows programming of up to ten temperature steps.

The facility is equipped with three ionization gauges, a quadrupole mass spectrometer and a capacitance manometer (MKS BARATRON, range ~ 100-10^{-3} Pa).

The quadrupole control unit is interfaced with a computer for the acquisition of the measurements.

The facility is also provided with a gas inlet system for quadrupole calibration, which is performed by introducing known gases into the measuring chamber at known pressure (10^{-3} to 10^{-5} Pa) and recording the quadrupole mass spectrometer signal.

All the facility components, including all gate valves, exposed to vacuum are metal sealed and can be baked up to 573-673 K, with the exception of the electrical feedthroughs of the coil, which have viton "o" rings and can be baked to 473 K only.

3. Samples and their pre-treatment

About twenty parallelepiped-shaped samples (0.02x0.02x0.005 m) were machined from blocks of SEP CARB B 112 and DUNLOP V graphites. In each of them two small tantalum tubes were inserted as described in Sect. 2.

The samples were then marked and cleaned and their whole surface polished with abrasive paper. Both during and after cleaning, gloves or pliers were used to handle the samples.

Four samples were tested without any heating pre-treatment, the remaining were pre-treated in a vacuum furnace at 1273 K for 20 h.

All pre-treated samples were exposed to air for two weeks before the outgassing tests.

4. Quadrupole calibration

Calibration of the quadrupole is required to obtain quantitative partial pressure measurements. The aim of the calibration is to determine the experimental sensitivity factor of the instrument, defined as the ratio of the quadrupole current signal Ix (the highest ion peak) of the gas x to the pressure Px of the same gas:

$$Sx = Ix/Px. \tag{1}$$

Calibration tests were performed using both the static and the dynamic method utilizing four different gases (H_2, CH_4, N_2, Ar) at a pressure of 4×10^{-5}–4×10^{-3} Pa.

In the static method, a known amount of the calibration gas was introduced in the measuring chamber after closing the pumping system. The amount of gas had been pre-determined by filling a small known volume (Fig. 1, item C) and measuring its pressure with a capacitance manometer (Fig. 1, item B) before pouring the gas into the measurement chamber. The absolute pressure in the measuring chamber was calculated according to the following formula:

$$Pc = Pv \cdot V1/(V1+V2) = Pv/788, \quad (2)$$

where:

Pc = absolute pressure of the calibration gas in the measuring chamber (Pa),

Pv = absolute pressure in the small known volume (Pa),

V1 = 5.5×10^{-5} small known volume (m^3),

V2 = 4.33×10^{-2} volume of the measuring chamber (m^3).

At each constant pressure in the chamber, the quadrupole current signal and ionization pressure were recorded.

The calibration tests based on this method were repeated several times. From the results we observe the following characteristics:

a) the dispersion of the results is so high that it is not possible to establish with sufficient certainty the trend of the sensitivity as a function of the pressure;

b) the sensitivity level of the quadrupole decreased constantly between one run of tests and the a subsequent run;

c) It takes such as a long time (at least one working day) to perform a complete run of tests that it was very difficult to make a sufficiently high number of tests for a statistical basis.

The second method consisted in introducing the calibration gas through a metering valve into the continuously pumped measuring chamber.

The quadrupole current signal was recorded at each constant pressure measured in the chamber by an ionization gauge, which was previously calibrated for each gas, exploiting the relation between the absolute pressure evaluated with the capacitance manometer and the pressure measured with the ionization gauge. For each gas, ten pressure-quadrupole signal series of measurements were performed in the range of $4\times10^{-6}\times4\times10^{-3}$ Pa.

This method compared with the static method has the following characteristics:

d) the tests can be done more quickly, so it was possible to make a large number of measurements for a wider statistical basis;

e) the measurements obtained have a lower dispersion of results (within ±30%);

f) the sensitivity level found with this method is lower.

The quicker method of testing, which allowed seven complete runs of measurements for each gas in a reasonable time, and the lower dispersion of results made it possible to find, with a better accuracy, a reference dynamics average sensitivity-pressure curve for each gas.

The sensitivity curve used to calculate the partial pressure was derived from the reference dynamic calibration curve corrected by a factor equal to the ratio between the reference sensitivity and that of the last calibration performed just before an outgassing test of a sample.

The conversion from the quadrupole signal to partial pressure is direct for those gases for which the calibration has been performed; for the other gases, sensitivity curves are calculated assuming as reference the available experimental curve of the gas with the closest mass and considering the following three parameters: fragmentation factor, ionization probability and transmission factor.

To obtain the calculated sensitivity curves, the following relations were used:

$$Sx = K \cdot Sy \tag{3}$$

$$K = (Fx/Fy)(\sigma x/\sigma y)(Tx/Ty) \tag{4}$$

$$Tx/Ty = My/Mx \tag{5}$$

where:

Sx = sensitivity of the gas x to be calculated;

Sy = sensitivity of the reference gas y with the closest mass to that of the gas x;

Fx = fragmentation factor of the gas x ;

Fy = fragmentation factor of the reference gas y ;

σx = relative ionization probability factor of the gas x respect to N_2;

σy = relative ionization probability factor of the reference gas y respect to N_2;

Tx = transmission factor of the gas x;

Ty = transmission factor of the reference gas y;

Mx = mass of the gas x;

My = mass of the reference gas y.

The fragmentation, relative ionization probability and transmission factors have been taken from the "Inficon Quadrex 200" residual gas analyser technical manual [1].

5. Evaluation of the outgassing rate

The evaluation of the outgassing rate depends on the method used for measurements.

a) In the "pressure rise method", the outgassing measurement tests are done closing the pumping system and simultaneously recording the quadrupole current signal and total pressure rise as function of time.

   The quadrupole current rate is calculated from the derivative of the quadrupole signal as function of time, and then converted into partial pressure rate, according to Sect. 4.

   The outgassing rates are calculated multiplying the partial pressure rates by the measuring chamber volume.

b) In the known conductance method, the outgassing rate is calculated measuring the partial pressure and taking into account the effective pumping speed for each gas in the chamber, according to the following formulas

$$Q = S_{eff} \times P \tag{6}$$

$$1/S_{eff} = 1/S + 1/C \tag{7}$$

$$1/C = 1/C_1 + 1/C_2 \tag{8}$$

where

Q = outgassing rate (Pa m^3/s)

S_{eff} = effective pumping speed in the measuring chamber (m^3/s)

P = partial pressure in the measuring chamber (Pa)

C = total conductance between the turbo and the measuring chamber (m^3/s)

C_1 = known conductance of the diaphragm (m^3/s)

C_2 = conductance of the by-pass pipeline (m^3/s)

S = 0.5 = nominal pumping speed of the turbo (m^3/s).

The conductances C_1 ad C_2 are calculated using the following relations:

$$C_1 = \pi/4 \times d^2 \times (RT/2\pi M)^{1/2} \tag{9}$$

$$C_2 = \pi/3 \times D^3/L \times (RT/2\pi M)^{1/2} \tag{10}$$

where

C_1 = known conductance of the diaphragm (m^3/s)

d = 10^{-2} = orefice diameter of the diaphragm (m)

R = 8,314 = molar gas constant ($Jxmol^{-1}xK^{-1}$)

T = 293 = absolute temperature of the gas (K)

M = molar mass ($kgxmol^{-1}$)

D = diameter of the by-pass pipeline (m)

L = length of the by-pass pipeline (m)

In the conductance calculation the absolute temperature T of the gas was taken equal to the room temperature considering that the molecules of the gas before entering the diaphragm are thermalized to the by-pass wall temperature (high number of collisions with the walls).

With reference to the formula (7) the effective pumping speed S_{eff} depends on the turbo pumping speed which is not constant for all gases. Nevertheless, considering that the ratio 1/S is much smaller that 1/C, the influence of the S variation on the S_{eff} value is very small and it can be neglected.

6. Outgassing tests

Before starting outgassing measurements of the samples, a characterization of the measuring chamber was performed by measuring its outgassing rate to get the background level. Since the measuring chamber is heated by the sample radiation, its background was measured at different temperatures. At the maximum temperature of the sample (1873 K), the temperature measured on the chamber walls was 353 K.

Dynamic quadrupole calibration has been performed before testing each sample.

Preliminary outgassing measurement tests were done at each constant temperature step using the pressure rise method.

The samples were heated up to 1873 K in steps of 200 K with a temperature ramp of 100 K per minute.

The preliminary tests have shown the limits in reproducibility of the results of the pressure rise method.

In fact, when the sample temperature increases following a temperature ramp the outgassing rate also increases.

Once the pre-programmed temperature has been reached, the outgassing rate initially shows a maximum peak and afterwords exponentially decreases, even if the sample temperature remains constant.

The difference between the maximum peak value and the stabilized value may reach a decade of pressure.

As consequence, the measured outgassing rate depends on the time elapsed between reaching the stable temperature and doing the test.

On the other hand, waiting for a stable pressure means measuring a lower outgassing rate than that corresponding to the maximum value.

Since the test requires several manual operations, there is uncertainty in the time reproducibility, which influences the outgassing measurement reproducibility.

In addition, another defect of the pressure rise method is that it does not allow outgassing measurements as function of time.

To overcome these problems, for subsequent measurements both "known conductance" and "pressure rise" methods have been used.

The first has been employed during all heating cycle, the second immediately after at stabilized temperature.

The heating cycle of the sample, which lasted a total time of 3600 s, was done with a temperature ramp of 200 K per minute followed by a soak.

In figures from 2 and 3 typical diagrams of the outgassing rates measured with the known conductance method are shown.

The outgassing rates values are net since the background corresponding to the temperature of the chamber has been substracted.

The most abundant gaseous species measured were H_2, CH_4, H_2O, CO, CO_2.

7. Conclusions

The outgassing measurements performed using the known conductance method have shown a good reproducibility of the results.

The tests carried out on two different materials have shown that the differences on the outgassing behaviour between SEP CARB N112 and DUNLOP V are negligible.

On the contrary, more meaningful are the differences between non-pre-treated and pre-treated samples.

An important phenomenon can be observed at temperatures between 1473 and 1673 K.

In this range of temperature the diagrams clearly show a sudden drop of the H_2O partial pressure with a correspondent increase of H_2, CO, CH_4, and CO_2 partial pressures.

In samples tested up to 1873 K the measured H_2O flow rate was even negative in the sense that the partial pressure was lower than that of the chamber background.

The drop of the water partial pressure and the increase of the H_2, CH_4, CO and CO_2 is due to the chemical reactions between C and H_2O.

Reference

[1] "Inficon Quadrex 200" residual gas analyser technical manual. Theory and interpretation.

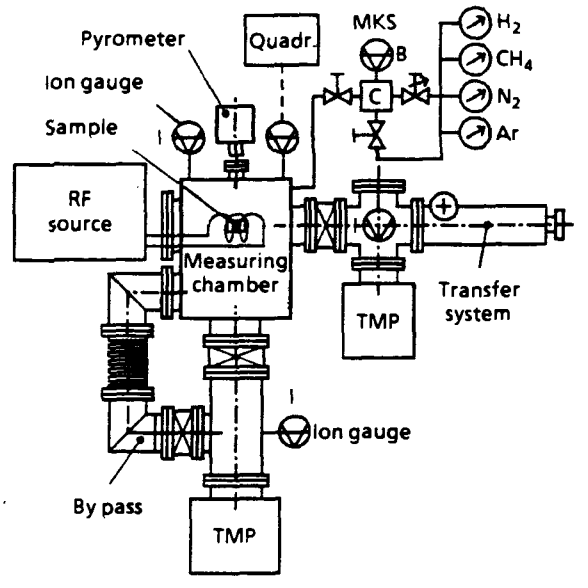

Fig. 1 - Schematic of the outgassing facility.

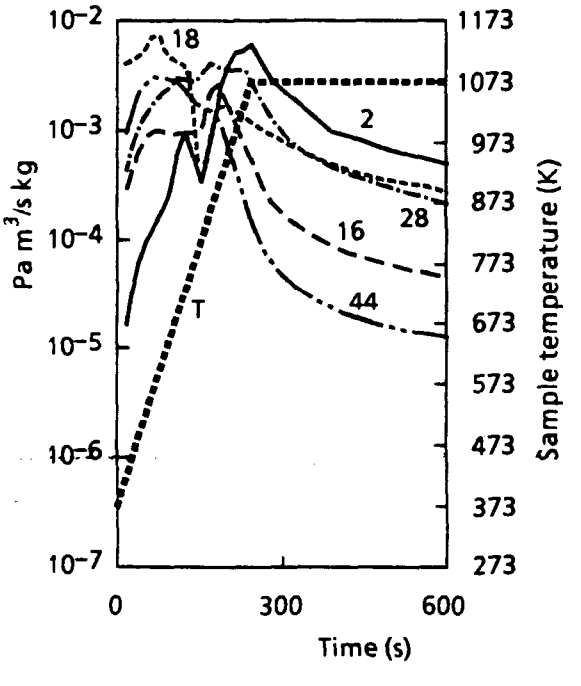

Fig. 2 - Non-pretreated SEP CARB N112 sample.

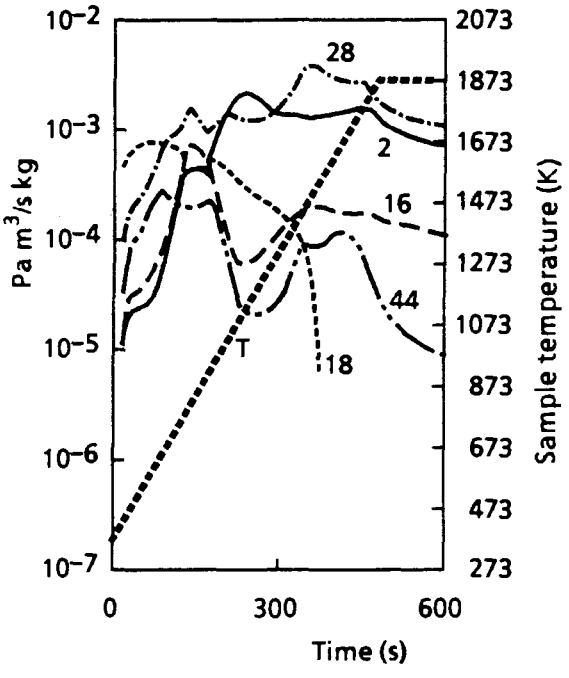

Fig. 3 - Pretreated SEP CARB N112 sample.

SILICON DEPOSITION ON STAINLESS STEEL SURFACES IN VIEW OF THE CONDITIONING OF FTU VACUUM CHAMBER

M.L.Apicella[1], M.G.Cicala[2], A.Neri[1], G.Traversari[1]
[1] Associazione EURATOM – ENEA sulla Fusione, C.R.E. Frascati, P.O. Box 65 - 00044 Frascati, Rome, Italy
[2] Centro di Studio per la Chimica dei Plasmi, CNR, Dipartimento di Chimica, Bari, Italy

ABSTRACT

The properties of silicon films deposited on stainless steel surfaces held at 77K, which is approximately the FTU (Frascati Tokamak Upgrade) wall temperature, have been investigated for the first time.

Bad adherence and traces of peeling have been achieved by using the same experimental conditions foreseen for the machine: silane concentration in helium equal to (0.11÷0.13) , current density in the range (40÷150)mA/m^2.

On the contrary, good results have been obtained on substrates held at 273K. This temperature represents a reasonable compromise for FTU operations.

1.Introduction

The use of silicon as first wall material in a tokamak has been attempted only very recently by the TEXTOR team (1). Silicon is very attractive because it forms tight bonds with oxygen, (which is one of the main light impurities in a tokamak discharge), and also more resistant to chemical erosion than other possible competing materials as boron.

The technique used for deposition of Si onto the tokamak walls is the plasma chemical deposition and it is analogous to that previously used for either carbonization or boronization. Indeed, it employs the same hardware with the only difference in the feeding gas: a mixture of helium with a minority of silane rather than methane or diborane.

The results obtained on TEXTOR - suppression of high-Z impurities, strong reduction of C and O and enhancement of the plasma density limit in comparison to the boronization case - are very encouraging also for FTU which has the first walls made of medium and high Z metals.

However, the peculiarity of the very low temperature of the FTU vacuum chamber, near 77K, makes it necessary a preliminary study of the quality of silicon films deposited on cold substrates.

This paper describes the properties of films deposited on stainless steel, of which are made the FTU walls, held at liquid nitrogen temperature, at 273K and at 298K. The 273K temperature has been examined since it is the highest value that can be reached on FTU walls by means the conventional heating techniques, still keeping cold the body of the machine.

In the following, the siliconization and desiliconization procedures are described. The characterization of silicon films, in terms of adherence and thickness, is presented, followed by an analysis of atomic composition performed by means of AES (Auger electron spectroscopy), SIMS (Secondary ion mass spectrometry), SNMS (Sputtered neutral mass spectrometry) and IR measurements. Finally we report our conclusions.

2.Siliconization

Hydrogenated amorphous silicon alloys (a-Si:H) have been extensively studied for the fabrication of thin films solar cells and for their application in the semiconductor industry (2). The plasma chemical deposition is generally performed on crystalline silicon or

quartz by means of a r.f. glow discharge (13,56 MHz) at high pressure (10-50)Pa of pure silane or silane diluted with hydrogen and temperature of the substrate in the range from 298 up 673K.

Our test, in turn, have been performed to simulate the same operative conditions foreseen for the machine: a dc glow discharge, low pressure $\sim$ 0.5Pa, low temperature of the walls (77-273)K and stainless steel as substrate.

The experimental apparatus is the same as used for carbonization tests (3) modified for the safe handling of hazardous gas such as silane. The chamber used for film deposition is a stainless steel toroidal sector of the FTU (r=0.333m), plus two covers with portholes for all the required equipment. A dc glow discharge is produced between a stainless steel central electrode and the grounded sector walls. A piezoelectric gas valve is used for the introduction of $He(80\%)+SiH_4(20\%)$ or $CF_4(90\%)+O_2(10\%)$, for siliconization and desiliconization respectively and for the introduction of H_2 or $He(90\%)+O_2(10\%)$ as required for the execution of the experimental tests (see section 5). All these gas mixtures are previously prepared in pressure bottles with the desired composition. Lower silane concentrations are obtained by adding He into the SiH_4/He gas before the introduction into the chamber.

Before each run, two different set of samples of SS 304, the same as used on FTU, are inserted close to the chamber walls. One is held at room temperature, as the deposition chamber, while the other is cooled to 77K or 273K during siliconization, by using liquid nitrogen or ice in equilibrium with water. Before each deposition the vacuum chamber and the samples are heated in vacuum at 423K for about two days.

In Table.1, the thickness d of the films produced after three different Si deposition runs are shown. Here J indicate the average density current on the chamber walls and Δt is the discharge time.

The experimental tests have been performed at 0.5Pa with a silane concentration of $P(SiH_4)/P(He)=0.11$, except the third one characterized by an higher value (0.13).

The film thickness, estimated by the difference of weight after and before siliconization, was higher for 77K samples than for 298K samples.

This growth rate enhancement of about a factor 2.5 is thought to be caused by an increase in the effective sticking probability of gas phase products.

On the contrary, the films deposited at 273K, presented the same thickness of samples deposited at 298K, as evidenced also by the same interference colours. No thickness evaluation was possible for the 77K

sample deposited in the first test because it was partially detached from the substrate.

The behaviour of the main molecular species in the gaseous phase was studied by monitoring their current intensity by a quadrupole mass analyzer (QMA).

In Fig.1 are shown typical spectra, obtained before (OFF) and during (ON) G.D.. The second spectrum is multiplied by 10 from mass 5 up to 35 for an easier comparison with the first one. Note that the QMA does not detect silane, when the discharge is switched off, but the radicals SiH_2(30), SiH_3(31), SiH(29), Si(28) and the gases H_2(2), H(1) produced by means dissociative-ionization processes which take place on the QMA filament itself.

In the "ON" phase the silane radicals (masses 29,30,31) are about a factor 10 lower than in the "OFF" phase, while the decrease of the Si mass is less pronounced. On the contrary the amount of H_2 is significantly higher. The decrease of 28,29,30,31 masses is due to the consumption of silane caused by dissociative-ionization processes similar to these occurring in the QMA: indeed the energies required for these reactions are lower than the ionization potential of the helium gas (24.5eV) which sustains the discharge. The different behaviour of Si respect to silane radicals is most probably due to an enhanced production of CO , which has the same mass as Si, inside the QMA chamber.

The increase of H_2 pressure, instead, is due to the cracking of the silane molecule which represents a source term for its production.

The higher voltages (> 600V), necessary to sustain the discharge for increasing silane concentrations, suggest that the plasma becomes more resistive as a consequence of the loss of energy of the electrons responsible for these reactions.

3. Desiliconization

Desiliconization was performed by means of a glow discharge with a mixture of CF_4(90%)+O_2(10%) (4) for the production of volatile compounds as SiF_4, CO and CO_2. About 3h at 100mA/m^2 of current density, were sufficient to clean off the 190nm thick silicon film deposited in 4h at room temperature.

To minimize fluorine implanted in the chamber wall the desiliconization was followed by a glow discharge in H_2 for 4h and subsequently by the baking at 423K for further 32h.

4. Characterization of the films

All the deposited films show interference colours similar to those of a-C:H films (3) indicating that they are semitransparent.

The layer thickness was measured, as described in section 2, assuming a silicon density of $2.2 \cdot 10^3$ kg/m^3 (2).

The measurement performed by the difference of level between a coated and a protected part of the sample was not possible because the films are very thin respect to the average depth of the groves on the substrate surface ($\sim 10^3$ nm).

All the films of the Table1 deposited at 77K were of very bad quality. Trace of peeling was detected on the substrates after they had been stored in air for 1 day. All these films were easily detached from the substrate simply by using a commercially available adhesive tape. Not only the adherence, but also the film quality was very unsatisfactory, as evidenced by the fine powder left on a paper pad after a mechanical wiping of the surface.

On the contrary, good films were obtained on the 298 and 273K substrates. No traces of peeling were observed under a microscopical analysis with a 320 magnification which revealed only the structure of the metal substrate.

The adherence of these films was evaluated by applying a traction force between the substrate and the film, which had been previously pasted to a metal sample. The adherence was higher than $280 \cdot 10^4$ kg/m^2, which is the limit for the breaking of the paste.

This adherence did not deteriorated by applying, under vacuum, a strong thermal stress to these films from the room temperature up to the nitrogen temperature. Three thermal cycles have been performed and no damage of the films has been observed.

5. Surface analysis

Firstly, the chemical reactivity to molecular oxygen of the film was established by measuring the amount of water in the silicon coated vacuum chamber after it had been exposed to the air for 24h.

The H_2O partial pressure detected by the QMA after evacuation of the chamber was higher than a factor 10 with respect to the value measured before film deposition. This behaviour contrasts with similar tests performed with carbon coated walls (3) which revealed a very low reactivity to the molecular oxygen.

The capability of the film to form tight bonds with respect to the ionized oxygen was tested by oxidizing the silicon coated walls by a G.D. in He(90%)+O_2(10%) for half an hour and then by exposing them to a G.D. in H_2 at high density current (150mA/m^2) to evaluate the production of H_2O or O_2 on QMA.

The following results have been obtained:

- a very long time ($\sim$ 15h) of G.D. was necessary to reduce the residual partial pressures of H_2O and O_2 of a factor 1.7 and 2.5 respectively.
- O_2 was the higher signal detected on QMA when the discharge was switched on, pointing out that the main mechanism of oxygen release is represented by ion impact desorption.
- silicon forms very tight bonds with oxygen which are very resistant to chemical erosion due to hydrogen ions. Indeed more than 12 hours of G.D. were needed to show the first signals of Si-H reactions as SiH_4 on the QMA. These reactions are believed to occur only after the consumption of the absorbed O. This is supported by the absence of erosion of the silicon coating after 15h of G.D., as observed by the interference colours of the vacuum chamber.

The atomic composition of the films was studied by means of AES and SIMS as a function of the distance from the surface, removing the deposited material with Ar ion beam.

Very similar results for 298 and 273K samples have been obtained.

A typical depth profile performed by Auger analysis on the 273K sample, after 1 month of exposureto air, is shown in Fig.2. Silicon with low traces of C and O are observed along the whole film thickness. The interface is very broad and significant amounts of silicon are found deep inside the substrate. On the contrary, a less broad interface and a strong oxidation of the film is observed at 77K, as evidenced by the deformation of the Auger spectral lines shifted at higher energies.

These experimental findings suggest that stable films, with a good adherence to the substrate, have been obtained only at 273 and 298K.

Also SIMS analysis confirms that Si is nearly constant in the films and, on crossing the interface, decays away. Very low hydrogen signal is detected into the films, but no evaluation of the atomic concentration is possible because this technique is not quantitative.

The presence of oxygen into the 77K sample has been observed by means SNMS technique more sensitive than SIMS to the presence of O (mass 16) and SiO (mass 44). A typical spectrum taken just at the film substrate interface for 77K sample is shown in Fig.3.

All the main component of the SS substrate ($^{52}Cr^{+}$,$^{56}Fe^{+}$,$^{58}Ni^{+}$) are observed together with $Si^{+}(28)$,$Si^{++}(14)$, $SiO^{+}(44)$,$O^{+}(16)$ and masses as $H^{+}(1)$ and $Ar^{+}(40)$. No traces of He at mass 4 are detected.

Additional informations have been obtained by means infrared measurements for the identifications of chemical bonds inside the films deposited at 298K and 77K.

Silicon substrates with very smoothed surfaces were used for their transparency to the infrared radiation.

In the Fig.4 the absorption spectrum obtained for 77K sample is shown. Here the typical vibrational modes of SiH_2 and SiH bonds are present, as normally observed in amorphous hydrogenated silicon films. In particular the SiO bonds is visible at 1078 cm^{-1}.

Apart from this peak, which is absent in the 298K film, a very similar spectra have been obtained at the two different temperatures.

The presence of oxygen on 77K sample does not affect the quality of the film which reveals good adherence without defects, as peeling or blistering.

6. Conclusions

All the experimental findings point out the critical role played by the substrate material for the silicon deposition at nitrogen temperature.

The poor adherence on stainless steel suggests that very weak chemical bonds are formed at the substrate film interface which affect the film growth. A very porous and instable film is produced which becomes, after air exposure, completely oxidized.

The good results obtained at 273K support the hypothesis that too low thermal energies are involved at 77K to activate film formation.

Acknowledgements. The authors wish to thank R. Belardinelli for its precious technical assistance.

References

(1) J. Winter et al., in : Proc. of the 20th Conference on Controlled Fusion and Plasma Physics, Lisbon, Portugal, 26-30 July 1993.

(2) M. Konuma, in: Film Deposition by Plasma Techniques, Springer Series on Atoms and Plasmas (Springer-Verlag,New York,1992)

(3) M.L. Apicella et al.,J. Nucl. Mater. 196-198 (1992) 549

(4) J.W.Coburn, in: Plasma Chemistry and Plasma Processing, Vol.2, No.1 (Plenum Publishing Corporation 1982),p.1.

Table 1 - Film thickness obtained after three different siliconizations

T	J=150 mA/m² Δt=4h (1)	J=75 mA/m² Δt = 4h (2)	J = 40 mA/m² Δt=6.5 h (3)
77 K	--	400 nm	700 nm
273 K		140 nm	
298 K	190 nm	140 nm	280 nm

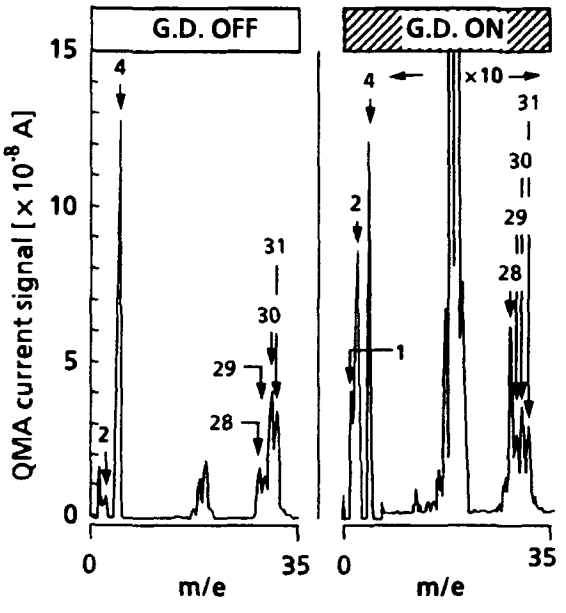

Fig. 1 - QMA spectra during and after siliconization. G.D. ON and G.D. OFF refer to the phased when the discharge is active (ON) or is switched off (OFF).

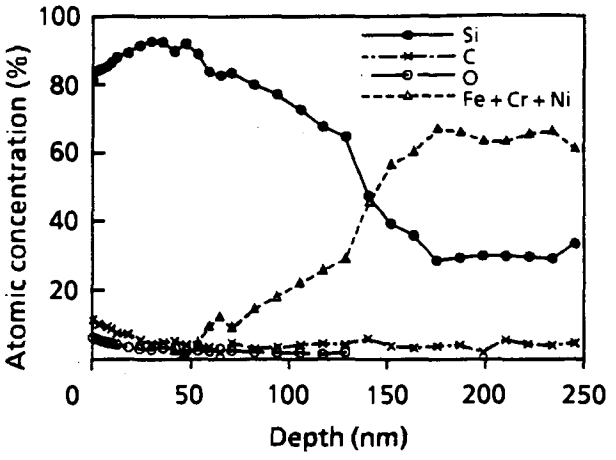

Fig. 2 - AES depth profile of Si, O, C and Fe + Cr + Ni for a 273 K sample.

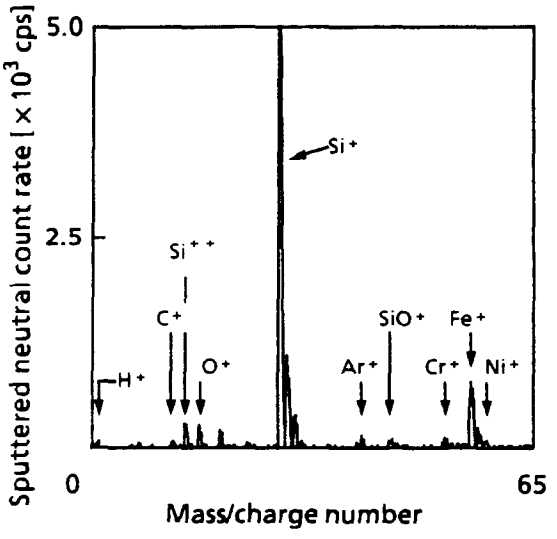

Fig. 3 - SNMS spectrum at the film substrate-interface for a 77 K sample.

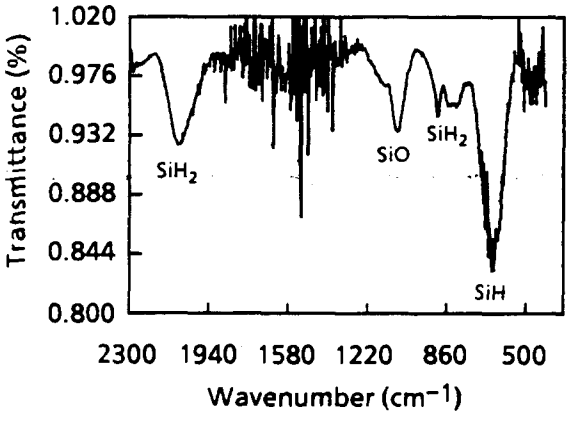

Fig. 4 - Infrared spectrum of silicon film deposited on crystalline silicon at 77 K. The ordinate represents the percentage of the transmitted radiation.

The 14 MeV Frascati Neutron Generator

M. Martone, M. Angelone, M. Pillon

Associazione Euratom-ENEA sulla Fusione
C.E. Frascati, Via E. Fermi 27, 00044 Frascati (Rome) Italy

Abstract

The 14 MeV Frascati Neutron Generator (F.N.G.) uses the T(d,n)α fusion reaction to produce $5.0*10^{11}$ n/s. In F.N.G. a beam of deuterons is accelerated up to 300 KeV by means of a linear electrostatic tube and directed onto a titanium tritiated target containing $3.7*10^{11}$ Bq of tritium. This paper describes the F.N.G. facility and its auxiliary apparatus as well as the neutron source calibration performed using the associated α-particle method.

1.0 Introduction

The 14 MeV Frascati Neutron Generator (F.N.G.) is a neutron generator based on the T(d,n)α fusion reaction. It was designed and built at the ENEA Energy Center of Frascati for conducting neutronics experiments in the frame of the research activity on Controlled Thermonuclear Fusion.

The neutronic design of blankets and shields of next step fusion devices requires to ascertain that the neutron cross section data sets used in the calculations are as accurate as possible and that the calculational methods used to transport the neutrons are as reliable as practical.

To ensure that both these criteria are met a suitable experimental activity (benchmark experiments) will be conducted at ENEA Energy Center of Frascati using FNG. Further FNG's applications will concern the development of a reliable instrumentation to control the ignited plasma, the measurement of activaction cross sections for dosimetric applications and other scientific as well as industrial applications (i.e. fast neutron analysis).

This paper describes FNG, its main components and auxiliary systems. The results concerning a first benchmark experiment performed using SS-316 are reported in a companion paper /1/ presented at this conference.

2.0 The F.N.G. facility

FNG uses the T(d,n)α nuclear fusion reaction to produce a nearly isotropic source of $5.0*10^{11}$, 14 MeV neutrons/sec. In FNG (Fig.1) a mixed beam of atomic and molecular deuterium ions is produced by a duoplasmatron ion source

and analyzed by a 90-deg bending magnet. Only monoatomic deuterium ions are sent into a uniform gradient accelerating tube and accelerated up to an energy of 300 keV. The beam is then focussed onto a tritiated titanium target by means of a magnetic quadrupole triplet. The ion source together with the 90-deg bending magnet and their associated electronics are held at high voltage potential and housed in two different high voltage terminals. The quadrupole triplet, the vacuum pump station and the target are grounded. The control signals and the current/voltage reading are transmitted to the control room through glass fibers.

Under beam bombardament, because of sputtering, some tritium is released into the vacuum system. A Vacuum Exhaust Clean-up Unit (VECU) was provided to remove this tritium from the vacuum exhaust. Tritium monitoring and control is obtained by means of four detectors as reported in sect. 3.

The neutron source strength is absolutely determined by counting the α-particle associated with the neutron produced by the D-T reaction. The α-particle are counted by means of a small silicon surface detector incorporated in the beam line. The uncertainty on the source strength measurement results lower than 4% at 1 σ level.

The FNG facility is housed in a large shielded hall (11.5 * 12 m^2 and 9 m high). For this reason it is particularly suited for conducting neutronics experiments like benchmarks which require low neutron return from the walls. The FNG design and present parameters are gathered in Table 1.

The FNG operation is assisted by several auxiliary systems which ensure personnel and machine safety. The most relevant are : the vacuum exhaust clean-up unit (VECU), the experimental-hall venting system, the target cooling system, the environment radiation-monitoring system and the control system.

2.1 Ion source and 90-deg bending magnet

The deuterium ions are produced in a duoplasmatron type ion source with expantion cup /2/. In this source a plasma is created in a vacuum vessel by means of a filament and an arc disharge. The plasma is confined by a combined geometric and magnetic effect and expands in a cup through a small hole in the anode. This allows to establish the best conditions for the extraction of the ion beam using a Pierce extraction electrode /3/. An electrostatic einzel lens /4/ is used to compensate for the residual beam expantion due to space charge effect before sending the beam into the 90-deg bending magnet. This is a sector shaped double-focussing magnet. The magnet is cut with a 40-deg edge angles and has a quite large air gap (80 mm) to ensure a large acceptance of the beam. Its uniform magnet field is 1.6 T which correspondes to a curvature radius of 22 cm for an energy-mass product of 60 keV*AMU. A 500 W stabilized power supply is used to control the magnetic field. Water cooling is used for winding pack and for vacuum wall hitted by the rejected molecular ions. The need for the bending magnet arise from the fact that the extracted beam contains D^+, D_2^+ and D_3^+ molecular ions. When hitting the target such molecular ions break into atomic ions each with 1/2 - 1/3 of the initial kinetic energy. At these low energies the neutron production rate is significantly reduced. Further, the molecular ions hitting the target increase the tritium sputtering rate which reduces the target lifetime while the tritium released into the vacuum system increases.

2.2 Acceleration tube and beam focalization

The acceleration tube is a 3 gaps uniform gradient type. The electrodes are reentrant for producing high field gradient in the evacuated tube, while the external field is low enough to allows the tube to be held in the open air. Two aluminum flanges at the tube ends provide the connection to the other FNG components. A multiple series of resistors strings in air with a current of 0.6 mA is used to distribute uniformily the electrostatic potential along the tube. The holding voltage is up to 300 kV. The high voltage power supply unit is a commercially SF_6 insulated Crockroft & Walton type with a maximum current of 10 mA.

The beam emerging from the accelerating tube is slightly diverging so a lens is needed to focus it onto the target. A quadrupole triplet is used at FNG. It has an aperture of 10 cm and a magnetic field of 1.5 kG. It allows to get a beam spot in the target of about 15 mm. The target is kept 2 m far from the accelerating tube end by means of a drift tube (Fig. 1). This is required to minimize the contribute of backscattered neutrons to the neutron source.

2.3 Target assembly

The F.N.G. target consists of a titanium tritide TiTx obtained by tritium absorbtion (260-330 GBq) in a titanium layer 4.4 μm thick. Titanium tritide is a stable chemical compound for temperatures lower than 200 °C at the FNG working pressure (10^{-3} Pa). The titanium layer is deposited on the bottom of a copper cup. The beam power (max 900 W) dissipated on the titanium tritide layer is removed by water flowing in a turbolent regime on the external

surface of the copper cup. This ensures the target temperature to be kept below 200 °C. Due to tritium diffusion some tritium could contaminate the cooling water. For this reason a closed loop containig 0.25 m^3 of water is used to cool the target.
The target is housed in a support designed to minimize the neutron scattering. The target support is insulated from the drift tube in order to measure the beam current on the target through a resistor. As a consequence the target is self-biased and secondary electrons suppressed.

3.0 The vacuum exhaust clean-up unit and radiation monitoring

Tritium is a radioactive element (β^+ emitter) with an half-life of 12.5 years. During FNG operation some tritium is released because of sputtering by deuteron bombardament and it is pumped away by the vacuum pumps. At the maximum power the tritium release from the target has been evaluated to be 37 GBq/h. A Vacuum Exhaust Clean-up Unit (VECU) was provided to remove the tritium from the vacuum exhaust in order to reduce the tritium release to the stack to 37 MBq/h. This is well below the maximum tritium release allowed (370 GBq/y) for FNG full operation.
The VECU operation consists on mixing the vacuum exhaust with dried air. The mixture passes through a low temperature (> 170 °C) catalytic bed for oxidizing the tritium to tritiated water. This water-vapour/gas mixture passes then through a molecular sieve where the water component is adsorbed. The whole system, whose lay-out is shown in Fig.2, is contained in a glove box located close to the generator. The VECU is controlled by the Control System which provides for its correct operation (recombiner temperature >170 °C, diluition air flow >0.2 l/min, vacuum exhaust pressure < 110 kPa).

The manipulation of tritiated target, as well as that of the various components for which a tritium contamination could be possible, is made by means of ventilated glove-boxes. A glove-box is intended for targets and radioactive waste storage, a second one is a movable glove-box suited to be fixed to the end part of the drift tube in order to avoid tritium contamination during target change.
Tritium monitoring is performed using four different detectors. One is located on the VECU exhaust line and is a 200 cm^3 γ-compensated ionization chamber. A second one is a 2000 cm^3 ionization chamber connected through a sequential sampler to the atmosphere of the glove boxes and of the ventilated box containing the target-cooling water tank. The third tritium counter (a gas flow proportional chamber, using pulse shape method to discriminate tritium from gammas /5/) is used for on line monitoring of the stack exhaust. The fourth monitor is also a stack exhaust monitor, but it is an off-line detector where tritium is absorbed in a pair of drier cartridges after its oxidation to tritiaded water. After water recovery, tritium is counted by standard liquid scintillation method.
Environment radiation monitoring during FNG operation uses commercial detectors. To measure the neutron and gamma-ray doses inside and outside the FNG building, three pairs of ^3He rem counters and proportional chambers with a sensitivity of 0.24 cps/μSv/h and 1.8 cps/μSv/h respectively are used.

4.0 Source-strength calibration

The time dependent neutron emission is monitored by a silicon surface barrier detector (SSD), which counts the α-particle associated to the neutrons of the D-T reaction, and by a BF_3 rem-counter. The former also provides the

absolute neutron intensity. This is done by recording the number of the 3.6 MeV α-particle, emitted in a known solid angle and in a fixed direction, produced by the D-T fusion reaction. The silicon surface barrier detector is located inside the drift tube at a distance L=1820 +/- 3mm from the target and displaced at r=30 +/- 1 mm off the deuteron beam line. A collimator limits the acceptance cone angle ($\Delta\Omega_\alpha$) to (3.14707 +/- 0.01758 cm^2)10^{-7} Sr. A thin aluminum deposit on the detector surface (300 $\mu g/cm^2$) eliminates the large background due to the high yield of scattered deuterons.

The source strength (n/s) can be determined if the solid angle transformation factor (from the laboratory frame to the center of mass frame, also known as anisotropic correction factor R_α), for the observed alpha-particle emission angle θ_α, is known. R_α is dependent on the deuteron energy E_d as well as on the α-particle emission angle θ_α. The absolute total neutron yield Y is given by /6/ :

$$Y = (4\pi/\Delta\Omega_\alpha)\ C_\alpha\ R_\alpha(E_d, \theta_\alpha) \qquad <1>$$

where C_α is the true count rate of the α-particles detected by the SSD. R_α has been calculated following the method reported in /6/. This calculation requires the T(d,n)α cross section and has been performed as a function of the ion beam energy E_d and of the stopping power $(dE/dx)_T$ of the target. In Table 2 the R_α values for different E_d values and the actual emission angle θ_α = 179.1 are gathered.

The overall accuracy for the total source strength measurement results lower than 4% at 1 σ level.

An independent method to measure the source strength is based upon the $^{27}Al(n,\alpha)^{24}Na$ reaction. Its cross section around 14 MeV is well known and it is assumed to be a

standard. An aluminum disc (0.1 mm thick and 12,7 mm diameter) is activated at a distance D from the neutron source. Measuring the absolute reaction rate (using absolutely calibrated HPGe detectors), and using the reaction cross section as well as simple geometrical corrections (due to source-Al disc distance and dimensions), the neutron source intensity is measured with an uncertainty lower than 5% at 1 σ level. The results obtained agree well with those from the α-particle method. Last , but not least, the time dependent ratio between BF3 and α-particle detector is also routinely calculated for each irradiation, to verify the stability of the counters. Up to now this ratio resulted stable within +/- 3 %.

5.0 F.N.G. applications

FNG has been designed mainly to perform benchmark experiments /1/, but its characteristics makes it a flexible system to be emploied for several industrial as well as scientific applications. Some of them have been already investigated (activaction cross section measurements, fast activaction analysis) and are next to became operative.

References

/1/ P. Batistoni et al.: " The stainless steel bulk shielding benchmark experiment at FNG " This conference
/2/ T.S. Green, : Rep. Progr. Phys. 37(1974) 1257
/3/ J.R. Pierce : J. Apll. Phys. 11 (1940) 548
/4/ A. Adams, F.H. Read: J. Phys. E :Sci. Instr. 5(1972)150
/5/ F. Berthold : " Tritium-in-air measurements by pulse shape discrimination methods " in Radiation Risk Protection, Vol. III, pp. 1091-1094 - FS-84-35T, published by TUV Rheinland Editor, Cologne (1984)
/6/ T.R. Ferwell : Nucl. Instr. Meth. 61 (1968) 61

Table 1 - F.N.G. Parameters

	Design	Present
Beam energy (keV)	300	230
D^+ beam current at the target (mA)	3	1
Beam spot size at the target (mm)	15	15
14 MeV neutron intensity (s^{-1})	$5\ 10^{11}$	$1\ 10^{11}$
Tritium content in the target (Bq)	$3.7\ 10^{11}$	$3.7\ 10^{11}$
Target lifetime (h)	2	10

Table 2 - The anisotropic correction factor R_α

E_d (keV)	R_α
200	1.2239
230	1.2343
250	1.2405
280	1.2488
300	1.2533
320	1.2588

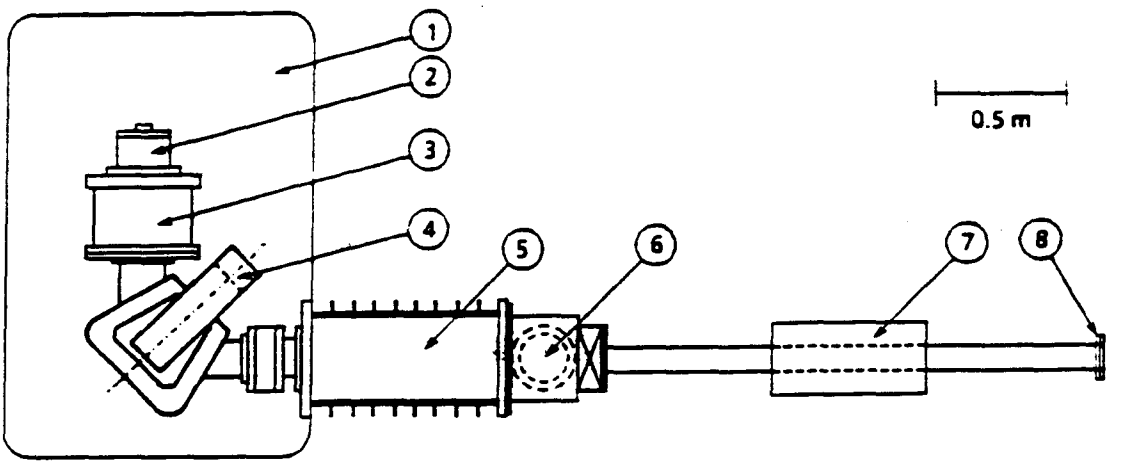

1-H.V. terminal
2- Ion source
3-Extraction optics
4-Bending magnet
5- Accelerating tube
6-Vacuum system
7-Q-lens
8-Target

Fig. 1 - The 14 MeV Frascati Neutron Generator main components.

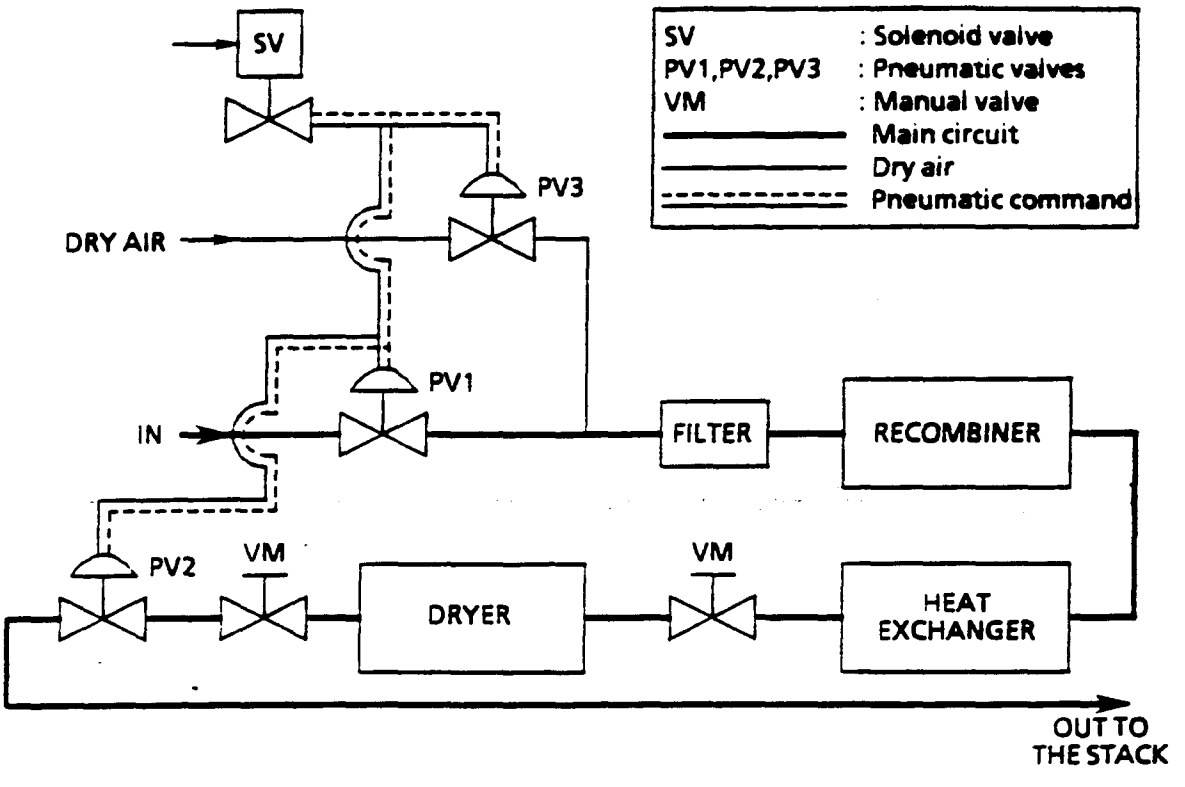

Fig. 2 - Lay-out of the Vacuum Exhaust Clean-up Unit (VECU).

Radiation Damage Calculations for Ignitor Components

S.Rollet[1], M. Zucchetti[2], P. Batistoni[1]

1 Associazione Euratom-ENEA sulla Fusione, Centro Ricerche Energia Frascati, C.P. 65, 00044 Frascati, Italy

2 Dipartimento di Energetica, Politecnico di Torino, C.so Duca degli Abruzzi 24, 10129 Torino, Italy

Abstract

Ignitor is a proposed high magnetic field tokamak aimed at reaching ignition conditions in a plasma of Deuterium-Tritium and at studying the physics of an ignited plasma for a period of a few seconds. Calculations of neutron and gamma fluxes have been performed, using both ANISN and MCNP codes. Particular care was dedicated for the zones closer to the plasma and for the components more prone to be affected by radiation damage. Given the calculated gamma and neutron fluxes, the integrated doses have been computed, using the SHAMSI library.

Neutron damage on the first wall and vacuum vessel is very small, both in terms of total dpa and of gas production. Due to the small fluence, Ignitor components appear to have no problems of neutron damage. The toroidal magnet insulator, is the only material for which the estimated damage is comparable with the maximum limit.

1 - Material problems for compact ignition tokamaks

One of the two main lines of development of tokamaks is the one dealing with high values of the magnetic field and small dimensions. These machines are therefore characterised by large values of the toroidal plasma current density, being this the ratio between the magnetic field and a linear dimension. A tight aspect ratio and an elongated confinement configuration go into this direction as well. High values of the poloidal magnetic field are also required, in order to achieve high plasma temperatures by ohmic heating. High field, small tokamaks must be very compact integrated structures, to stand the electromechanical stresses generated by high operational magnetic fields. They are characterised by high thermal and neutron loads, but low fluences. The blanket and the shield are missing.

The Ignitor-ULT tokamak [1-3], which will be taken as reference (see fig.1), consists in a plasma vacuum chamber, made of 12 INCONEL-625 welded sectors, covered by a first wall of graphite tiles . The toroidal field magnet consists of 24 D-shaped coils, each one encased by two C-shaped steel clamps, which are wedged together in their outer region. The C-clamps are prestressed by two shrink rings and forced to bend their noses towards the equatorial plane of the machine, applying an axial compressing force on the inner legs of the TF coils. An electromagnetic press, using the central post as the contrasting element, cooperates with the shrink rings. The poloidal field system is made of four sets of windings (ohmic heating, shaping, equilibrium and feedback), made by wound copper conductor. The machine is completely enclosed by a cryostat made of glass reinforced epoxy, as structural material, and plastic insulating foams. The machine is supported by eight legs, seismically designed. Making reference to the above listed components, which are typical of a compact ignition tokamak, a short summary of the main factors affecting the choice of their constituting materials will be carried out. A first design requirement, valid for

all material choices, is that no new or special material has to be employed (see Table I).

Concerning the first wall, which is in this case a set of protection tiles exposed to the plasma and covering the vessel, thermal loads under normal conditions and disruptions are the main design constraint. During normal operation, the plasma columns leans against the inner wall of the plasma chamber, which acts as a large-surface limiter, and receive most of the energy associated to the particles outflow. For Ignitor, heat loads around 3.5-4 MW/m^2 are considered. Moreover, peaking factors may derive from uncertainties in plasma physics and control. In a plasma disruption, all the plasma thermal energy (about 10 MJ) is deposited on the first wall in less than 1 ms. This produces instantaneous overheating, and wall erosion due to particles bombardment. Given this scenario, graphite is the best choice. Low atomic number, high thermal diffusivity, good mechanical properties, low ash content and low open porosity, good thermal shock behaviour are its main good characteristics. Beryllium, which has a lower atomic number and therefore is preferable from the point of view of plasma purity, has worst properties than graphite in all the other listed cases, and it is also a toxic material. Tritium retention in graphite and its possible reaction with hydrogen to form methane are the main drawbacks.

The plasma chamber (vessel) provides the high vacuum environment required for plasma operation, and is the main tritium confinement boundary. It supports all internal hardware (e.g., the first wall) and must resist the weight, the vacuum, the mechanical, thermal and electromagnetic operating loads, as well as the nuclear radiation from the plasma.

Concerning structural analysis, two load conditions affect the design requirements: a) atmospheric pressure and electromagnetic loads during normal operation b) plasma disruptions. Although the design of such machines is not regulated by specific Codes and Standards, ASME III guidelines can be followed

to identify the basic criteria for the stress limits. In case a), the loads considered are the outer pressure (0.1 MPa, versus an internal vacuum of $5*10^{-9}$ torr), and the magnetic pressure due to the interaction between the toroidal magnetic field and the poloidal currents induced in the chamber. The eddy currents induced by plasma motion and current decay during disruption generate the main loads in the chamber (case b). The loads generated in the most conservative scenarios (current collapses and vertical instability), lead to the choice of an alloy with better mechanical properties than steels.

Other design requirements concern the resistance to thermal cycles (fatigue) during plasma discharge from cryogenic temperature, and during baking phase and discharge cleaning process from room temperature up to 200-250 °C for vacuum conditioning. Weldability is important as well: due to the complex shape of the plasma chamber, postweld heat treatments are not possible. The Inconel alloy 625 is a Ni-Cr-Mo alloy, with Nb addiction that acts with the molybdenum to stiffen the alloy matrix and thereby to provide high strength without a strengthening heat treatment. It is a non magnetic alloy, with high strength and toughness from cryogenic temperatures up to 1000 °C, with a very high fatigue resistance. Inconel 625 plates show excellent weldability, without the need of postweld heat treatments. Concerning the mechanical properties at room temperature, Inconel 625 shows substantial advantages, compared with AISI 316LN: ultimate tensile strength (UTS) of 850 MPa vs. 600 MPa, yield strength (YS) of 420 MPa vs. 300 MPa, Young modulus of 215 MPa vs. 196.5 MPa etc.. Properties at cryogenic temperatures (UTS and YS) are better than those at room temperature.

The electromagnetic structure (magnetic field coils, TFC and PFC, and C clamps) are made of different grades of copper, and AISI 316LN. Concerning mechanical behaviour, three main factors have to be taken into account, i.e. mechanical progressive deformation, creep, and oligocycle fatigue. Progressive deformation may occur when the stresses in some copper conductors exceed the

yield point in limited areas. This may spoil the insulation, which is obliged to undergo the same plastic permanent residual as copper. Concerning creep, unfavourable stress situations (high load, slow cooling and load reversal) occur in some PFC, whereas TFC have no problem. However, a conveniently chosen grade of strain hardened Cu Oxygen-free (OF) can withstand the situation for PFC. Oligocycle fatigue, with a well shaken down structure and a ductile enough Cu OF, is measurable in thousands of cycles.

Concerning TFC, taken into account the previous point, and the very stringent requirements that physics considerations impose on the electric properties of the copper, the final choice for Ignitor has been the use of a convenient grade of high conductivity oxygen-free copper, with a very low phosphorus content (OFHC). The electrical resistivity of Cu OFHC bars is no more than 0.0123 $\mu\Omega$ cm at 4 K, 0.209 $\mu\Omega$ cm at 77 K and 1.72 $\mu\Omega$ cm at 295 K. Concerning PFC, Cu OFHC has been chosen for those coils in Ignitor where stress situations may lead to creep. Dispersion strengthened Cu (GlidCop Al-15 LOX) is used for the other ones.

For most of the mechanical structural components other than the vessel (C-clamps, central post, tensioning ring, reaction plates, supporting legs, see fig.1), AISI 316LN has been selected. Nitrogen addition (0.1 to 0.16%) increases both the ultimate and tensile strength values at room and at low temperature, while maintaining good toughness also at the foreseen service temperature (7.7 K). The insulating materials, whose mechanical properties are even more important than those of copper, will be a compound of boron-free high strength glass tissue and of a clorine-free low-N low-O epoxy, with very low viscosity and rather low curing temperature.

2 - The neutronic model of Ignitor-ULT

Some radiation damage problems of the above materials will be addressed in this paper, for the case of Ignitor-ULT machine whose major radius is R_0 = 130 cm and minor radiuses are a = 47 and b=87 cm. The reference operation agenda assumed in this work is given in Table II. Different operation scenarios are foreseen, with the neutron yield ranging from 10^{17} n/s in the low regime to 3 10^{19} n/s, leading to a neutron flux on the first wall up to 10^{14} n/s cm^2, comparable with that of a demonstration reactor.

In order to determine the neutron flux and hence the dose in each points of interest, a geometry model of Ignitor has been performed using both deterministic discrete ordinates neutron transport codes (ANISN) [4] and Monte-Carlo codes (MCNP) [5]. The early results of the flux calculation with the two codes are reported in Ref. [6].

More detail about comparison performed between 1-D and 3-D neutron flux calculation could be found in Ref. [7].

3 - Neutron damage assessment

Ignitor has no blanket and shield between the first wall and the magnets. Given the high neutron and gamma radiation field, certain components could be damaged and degrade their properties. Neutron damage effects on the first wall and vessel, on the magnet - insulating materials and on the cryostat materials may become relevant.

To verify the lifetime of the most critical components, neutron and gamma fluxes have been calculated in all the components, with particular care for the zones closer to the plasma and for the components more prone to be affected by radiation damage, like the toroidal magnet insulator or the cryostat walls. Given the calculated gamma and neutron fluxes, as described in the

previous section, the heat deposition rate and the integrated doses have been computed, using the SHAMSI library of kerma factors [8].

The annual operational neutron generation is of 3.7 10^{22} neutrons. The results of the neutron damage calculations are reported in Table III. The only component in which the dose is comparable to the limits is the insulator of the TFC: the annual integrated dose on the insulator turns out to be about 6.1 MGy/y: about 60% of the total dose is due to neutrons, while the remaining is due to gammas. Since some relevant detriment of insulator properties begins at 30 MGy (Ref. [9]), the foreseen three-year operation at DT of Ignitor-ULT should not require the substitution of this component.

The annual maximum integrated neutron dose on the insulator of the central transformer is about 0.43 MGy/y, then fully acceptable. The annual integrated neutron dose on the cryostat is 0.022 MGy/y, and it is therefore negligible. As far as the first wall and vessel are concerned, the neutron damage rate while the machine is working would lead to a value of about 26 dpa per year in Inconel 625. Ignitor is however a pulsed machine with an equivalent burning time of about 1000 full power seconds during one calendar year: then the total neutron damage on the Inconel 625 vessel due to three years of DT operation in Ignitor is less than 0.003 dpa, a negligible value. Also the gas production is negligible.

4 - A study for magnets radiation damage reduction

Due to the small fluence, Ignitor components appear to have no problems of neutron damage. The toroidal filed coils insulator, however, is the only material for which the estimated damage is comparable with the maximum limit. Minor modifications of the machine design in order to improve magnets shielding are discussed in this section. Calculations of the sensitivity of the neutron

damage on the TFC insulator to minor design modifications has been studied by means of ANISN neutronic models, similar to those described in section 2.

The most plain solution to improve magnet shielding is to increase the thickness of the vessel. This however has an impact on all the machine design and must be done with the greatest caution. Results of the ANISN runs show that the integrated annual dose on the TFC insulator (called DITFC from now on) can be reduced down to 5 MGy/y if the thickness of the inboard vessel is increased from 17 mm to 28 mm, and to 4.5 MGy/y is the thickness is of 37 mm.

Other solutions are however conceivable. Shielding capability of the vessel could be improved by the addition of B. It has been found that an addition of 1 wt% of natural B to INCONEL 625 would reduce the DITFC to 5.8 MGy/y. If B is totally enriched in B-10 then the DITFC is reduce to 5.6 MGy/y. About 60% of the DITFC is due to neutrons: neutron absorption in the vessel could be increased by a moderator, which, softening the spectrum, would increase thermal neutrons capture. In our case, this can be done by increasing the thickness of the graphite first wall. In fact, if the inboard first wall tiles pass from a thickness of 23 mm to a thickness of 34 mm, then the DITFC is reduced to 5.6 MGy/y, due to the increased neutron absorption in the vessel. If the thickness is of 45 mm, then DITFC is 5 MGy/y.

Best results are obtained combining the solutions: if the thickness of the vessel is increased of 1 cm and an addition of 1% of B-10 is made to INCONEL-625, then the DITFC is reduced to 4.8 MGy/y. If also the thickness of the graphite tiles is increased of 1 cm, then the DITFC is 4.3 MGy/y.

5 - Overview and conclusions

High magnetic field compact ignition tokamaks, like Ignitor-ULT, are characterised by high thermal and neutron load, but low fluences. First wall and vessel materials must withstand thermal loads under normal conditions and

during disruptions, as well as the electromagnetic loads. The electromagnetic structure, besides mechanical behaviour problem, as progressive deformations and creep, may have radiation damage problems. Ad hoc neutronics calculations have been performed to assess neutron damage behaviour at Ignitor components. It turned out that no problems are foreseen; the only case in which the response is near the limit is for the TFC insulator.

References

[1] B. Coppi, M. Nassi, L.E. Sugiyama, Fus. Tech. 21 (1992) 1607

[2] B. Coppi, L.E. Sugiyama, M. Nassi, Fus. Tech. 21 (1992) 1612

[3] B. Coppi, M. Nassi and the Ignitor Project Group, Characteristics of the Ignitor-ULT experiment, M.I.T. Report, PTP-92/8, (March 1993)

[4] W. W. Engle jr., A user's Manual for ANISN, ORNL K-1963, Oak Ridge Nat. Lab. (1967)

[5] J. Briesmeister (Ed.), MCNP: A General Purpose Monte Carlo Code for Neutron and Photon Transport, LA-7396-M (Revised Version 3A), Los Alamos National Laboratory, (1986)

[6] P. Batistoni, S. Ciattaglia, S.Rollet, M. Zucchetti, in Proc. Symp. Fus. Techn. SOFT 92, Elsevier SP (1992), 1281

[7] P. Batistoni, S. Rollet, M. Zucchetti, Report E.N.E.A. in progress (1993)

[8] C. Ponti, T. Abbas, "*SHAMSI*", EUR-12622 EN, Eur.Atom. En. Comm.(1982)

[9] ANSALDO-CERN Private Communication

Table I - Material composition of Ignitor components (the percents represent weight fractions)

Component	Material
First Wall	Graphite
Vacuum Vessel	Inconel 625
External TF Magnet	Cu OFHC (96%) + Insulator (4%)
Internal TF Magnet	Cu OFHC (98%) + Insulator (2%)
TF Magnet Insulator	Fiberglass (60%) + Insulator (40%)
Central Transformer	Cu OFHC (94%) + Insulator (6%)
Poloidal Coils	Glidcop (94%) + Insulator (6%)
Structural Materials	SS AISI316 LN
Shrink Rings	Inconel 718
Cryostat Wall	Polyuret. (90%) + Fiberglass (10%)
Coolant	Nitrogen

Table II - One year DT operation Agenda

Experiment Parameter	Low Regime	Intermediate Regime	Moderate Regime	High Regime	Extreme Regime
B_T Field (T)	5.5	8	10	11	13*
I_p Plasma Current (MA)	5	7.5	9	10.5	12*
Number of Discharges/Y	400	500	670	150	70
Neutron Yield (n/s)	$1.03\ 10^{17}$	$1.39\ 10^{18}$	$6.95\ 10^{18}$	$1.34\ 10^{19}$	$2.75\ 10^{19}$

(* Maximum values)

Table III - Neutron damage in Ignitor-ULT, due to one year of DT operation.

Component	Damage Parameter
TFC Insulator	6.14 MGy
Central Transformer Insulator (1)	0.43 MGy
Central Transformer Insulator (2)	0.18 MGy
Central Transformer Insulator (3)	0.04 MGy
Cryostat	0.022 MGy
Vessel	$8.3\ 10^{-4}$ dpa H=0.07 appm He=0.01 appm
First Wall	H<0.01 appm He=0.11 appm

(1) Maximum flux exposed; (2) Average flux exposed; (3) Minimum flux exposed

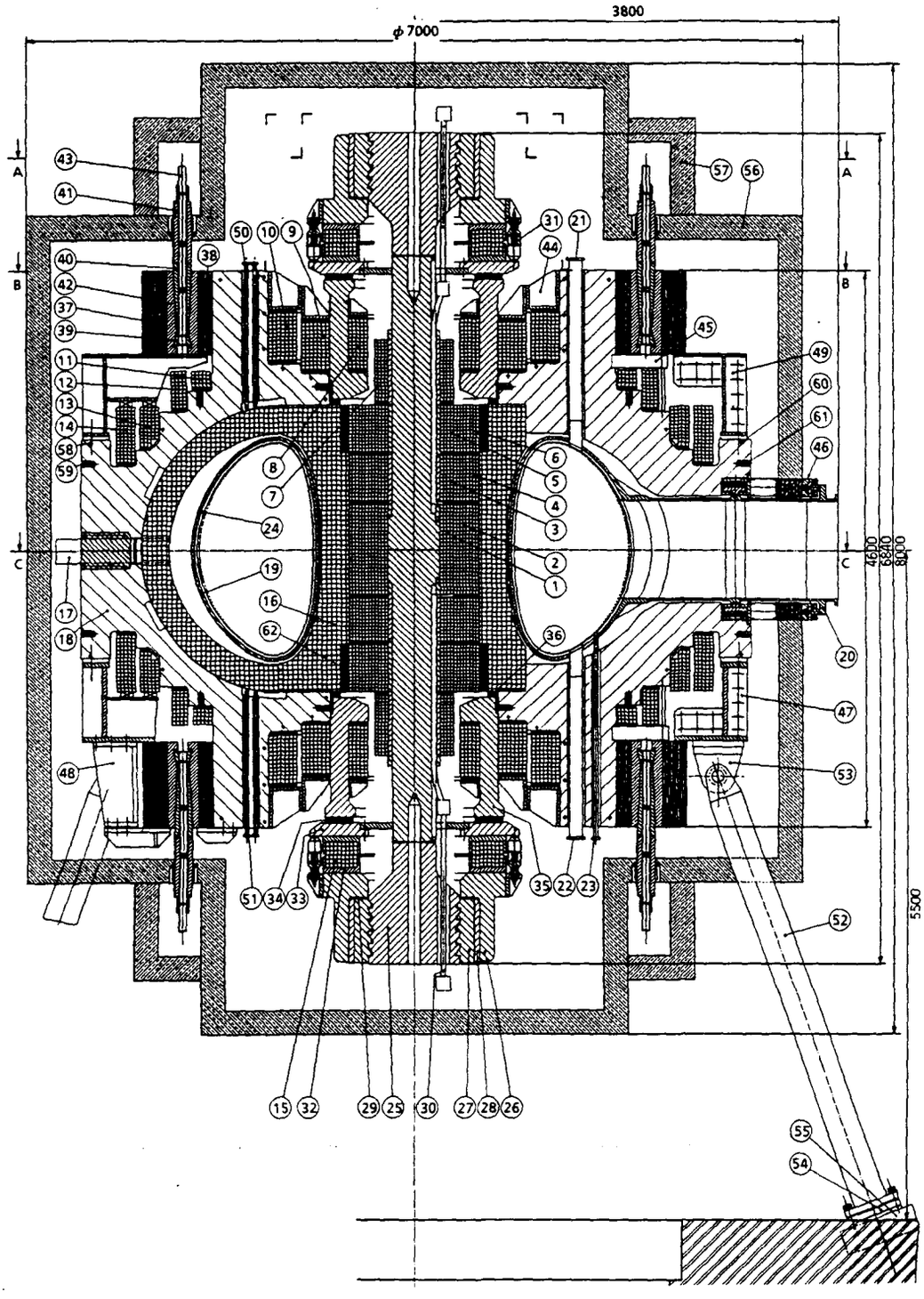
3800
φ 7000
A
B
C
4600
6840
8000
5500
43
41
40
42
37
39
38
50
10
9
31
21
44
57
56
11
12
13
14
58
59
8
7
24
19
16
62
17
18
6
5
4
3
2
1
36
45
49
60
61
46
20
47
53
48
51
34
33
35
22
23
52
15
32
29
25
30
27
28
26
55
54

LEGEND

1-14 Poloidal coils
15 Axial press coil
16 Toroidal magnet TF
17 TCF feeding connection
18 C-Clamp
19 Plasma chamber
20 Equatorial port
21-22 Diagnostic vertical ports
23 Gas injection vertical port
24 First wall
25 Center post
38 Fiberglass spacer
26 End bell
27 Groved sector
28 Locking sector
29 Shim
30 Feeding connctions
31 Elastic support
32 Press coil housing
33 Press load transfer ring
34 Press spacer
35 Piston
36 Piston spacer
37 Shrink ring
38 Fiberglass spacer
39-40 Tensioning wedge
41 Wedge extension
42 Reaction plates
43 Tie rod
44 Coil 9-10 support
45 Coil 11-12 support
46 Plasma chamber support
47 Support ring
48-49 Tensioning system support
50-51 Helium feed pipe
52 Support leg
53-54 Supports
55 Foundation plinth
59 Half sector dowel pin
60 30° sector assembling bolt
61 30° sector dowel pin
62 Coil armour ring

Fig. 1 - The Ignitor-ULT vertical cross-section

The stainless steel bulk shielding benchmark experiment at FNG

P. Batistoni[1], M. Angelone[1], M. Martone[1], L. Petrizzi[1], M. Pillon[1], V. Rado[1], A. Santamarina[2], I. Abidi[2], G. Gastaldi[2], P. Joyer[2], J.P. Marquette[2], M. Martini[2]

[1]Associazione EURATOM - ENEA sulla Fusione, C. R. E. Frascati, I-00044 Frascati, Rome, Italy

[2]Commissariat à l'Energie Atomique, Centre d'Etudes Nucleaires Cadarache, 13108 St.-Paul-lez-Durance, Cedex, France

Abstract

In the frame of the European Technology Program for NET/ITER, ENEA - Frascati and CEA - Cadarache in collaboration, are performing a bulk shielding benchmark experiment, using the 14 MeV Frascati Neutron Generator. The aim of the experiment is to obtain accurate experimental data for improving the nuclear data base and methods used in the shielding designs, through a rigorous analysis of the results. The experiment consists in the irradiation of a large SS-316 block by 14-MeV neutrons. The neutron fluxes and spectra at different depths, up to 65 cm inside the block, are measured by means of fission chambers and activation foils, characterized by different energy response ranges. Also the γ-ray dose measurements are performed with ionization chambers and Thermo-Luminescent Dosimeters. The first results are presented, as well as the comparison with calculations by the S_n code BISTRO and the Monte Carlo code MCNP, using the european JEF/EFF libraries.

1. Introduction

Due to the large neutron load on the first wall, NET/ITER will have a shielding blanket to reduce the neutron and photon fluxes at the outer components at acceptable levels. The thickness of the shielding blanket is limited by space and design constraints, but it must be sufficient to protect the toroidal magnetic field coils (TFC) against radiation damage and excessive nuclear heating. One of the proposed shielding material is stainless steel, whose performances have been largely analyzed by means of calculations of the total heat load and of local nuclear responses. However, such analyses must account for the uncertainties in the nuclear data, calculation methods and models, that result in an uncertainty on the minimum allowable shielding thickness. To reduce such uncertainties, the European Technology Program has promoted an activity of Benchmark Experiments aimed at obtaining accurate experimental nuclear data for shielding materials/configurations, for improving nuclear data base and methods through a rigorous analysis of the results.

In this framework, ENEA - Frascati and CEA - Cadarache in collaboration, are performing a Bulk Shielding Experiment (NET Task NDB2.1), using the 14 MeV Frascati Neutron Generator (FNG). This has been the first experiment performed at FNG, that started operations at the end of 1992. The description of FNG can be found on a companion paper presented at this conference [1].

2. Description of the experiment

For the first experimental assembly, a stainless steel (AISI316) block was chosen in a configuration allowing for deep penetration measurements of neutron and gamma flux. The block consists of 14 plates, each with an

extention of 100x100 cm^2 and a thickness of 5 cm, for a total block thickness of 70 cm. This configuration has been chosen as representative of the inboard shield of a fusion reactor. The block is positioned in front of the neutron source, at 5.3 cm from the tritiated target, and is located on a movable tower at 4 m from the floor (see Fig.1 in Ref.[2]) and at larger distances from the walls to reduce the neutron background due to room return. The block is provided with a central channel of 30 mm diameter to introduce rods of variable inner diameter, namely 18, 12 mm and 9 mm that serve for the location of the various detectors at different penetration depths. The detector channel is aligned with the beam propagation direction. To assess room return background in the FNG bunker, calculations have been performed using both BISTRO and MCNP codes. The results of the two calculations agree with the fact that the room background is negligible at any neutron energy, only beyond 7 cm inside the block.

3 - Experimental techniques

The foil activation technique has been employed, as in previous experiments, to determine the neutron flux at different depths inside the block. The main advantage of the activation method is that it provides accurate integrated flux values in the fundamental energy range for damage or coil heating, i.e. the 100 keV - 1 MeV range, where the flux tilts due to resonances introduce large uncertainties in spectrometric measurements. Moreover, this passive dosimetry method has the advantage that the small size of detector foils make good spatial resolution and little perturbation of the local field. Furthermore, the neutron spectra can be deduced by using multifoil detectors with different responses.

The activation measurements have been performed by the ENEA team. The selected activation reactions are listed in Table I, showing also the

corresponding sensitivity range (more measurements are in progress employing other activation reactions, i.e. $^{58}Ni(n,p)$, $^{58}Ni(n,2n)$ and $^{103}Rh(n,n')$). Foils of 18 mm diameter and various thicknesses (1-2 mm for Al, Fe, In and 50 -100 μm for Au and Mn) have been irradiated up to 61 cm of depth inside the block, with a source intensity close to 10^{11} n/s and for irradiation intervals ranging from 1 to 4 hours, depending on the reaction. The irradiation histories are recorded by two neutron flux monitors (α-detector and BF_3 counter) for the decay correction during the irradiation. After irradiation, the induced γ-ray activities are measured by two HPGe detectors whose absolute efficiency is previously determined by a set of well calibrated commercial sources. Intercalibration of the two detectors are performed both using calibrated sources as well as activation foils. The measured activities agree within the experimental uncertainties (±2%). The *nuclear data are taken from* Ref.[3].

The major sources of errors for the measured reaction rates are the γ-ray counting statistics, that range from ±1% to ±5% for almost all the measurements with the only exceptions of Al at 56 cm (±9%), and Fe at 61 cm(±15%), the uncertainties on the detector efficiency and finally, on the neutron source intensity which is less than 4% (see Ref. [1]). Other sources of errors such as those on decay constants, γ-ray branching ratios and on foil masses, are negligible.

Neutron flux measurements have been also performed by the CEA team using micro fission chambers, i.e. ^{237}Np (representative of DPA response function) and ^{235}U (thermal flux) chambers. These detectors have a cylindrical shape with an external diameter of 8 mm and a total length of 8 cm. They have been located at several penetration depths up to 65 cm, trough a 9 mm diameter channel inside the block. The absolute calibration of fission chambers, has been performed at Cadarache using the thermal neutron

column of the Harmony experimental reactor. Further measurements with a ^{238}U (fast flux) fission chamber are in progress.

The measured reaction rates, both for activation foils and for fission chambers, are shown in Fig.1, in units of reactions per 10^{24} nuclei and normalized to the total neutron yield Y_n. The corresponding total error bars are smaller than the adopted symbols.

Finally, ionization chambers and thermo-luminescent dosimeters have been used to measure the γ-ray flux inside the block. The ionization chambers had an external diameter of 11 mm, a length of 13 cm and a sensitivity of 10^{-13} A/(rad/h). Two different types of TLD have been used by two independent CEA experimental teams. Typical experimental errors, obtained in the first measurement campaign, are ±20% for TLDs and ±30% for ionization chambers.

4 - Calculational tools

The analytical interpretation of the experimental measurements is carried out by means of MCNP.4 code by the ENEA team and with the S_n BISTRO code by the CEA team. In both cases, the transport cross sections are originated from EFF.1 file.

The Monte Carlo simulation allows for an adequate representation of the experimental features and an accurate treatment of the neutron transport with continuous cross sections, so that the C/E comparison can be referably essentially to the basic nuclear data. The Monte Carlo simulation can also give an useful assessment of the 2-D multi-group S_n treatment, which has to be used in sensitivity and uncertainty analysis.

In MCNP, the detector responses are calculated in a model which represents the block, the close materials around the block and the detector devices. The room background contribution at the detector positions close to

the block walls is also estimated with a separate calculation representing the whole experimental environment, including the bunker walls.

An accurate description of the energy and angular distribution of the neutron source is made in MCNP, based on the reaction kinematics and taking into account the energy loss in tritium-titanium layer. A very stressed variance reduction is required to improve the statistical accuracy for the deep penetration and the slowing down effects. The weight-window technique is adopted by using an importance distribution which depends on space, energy and detector response. The importance functions are obtained by a set of 1-D S_n calculations. The representation of the exact activation foil geometry is requested for the low energy detectors (Au and Mn) for which the resonant self absorption effects are quite significant. For the all calculated responses the fractional standard deviation due to calculation statistics ranges from 1 to 4%. The activation reaction cross sections have been taken from different sources, i.e. $^{27}Al(n,\alpha)$, $^{55}Mn(n,\gamma)$, $^{56}Fe(n,p)$, $^{58}Ni(n,2n)$ and $^{58}Ni(n,p)$ from EFF.2, $^{115}In(n,n')$ from EAF.2, $^{103}Rh(n,n')$, $^{197}Au(n,\gamma)$, $^{235}U(n,f)$ and $^{237}Np(n,f)$ from JEF.2. The errors on the calculated reaction rate include the calculation statistics and the error due to the uncertainty on the activation cross section, when available, obtained with a variance analysis.

Deterministic neutron and gamma flux calculations have also been carried out by using the french S_n code system, the modular BISTRO package [4]. BISTRO solves the Boltzmann equation through various discretization schemes (Diamond, Step, "teta weighted", or Diamond + "teta weighted"). Iterations are accelerated by an efficient Diffusion Synthetic Acceleration (DSA) method. The multigroup cross section library is derived from MATXS-87 Library [5] by TRANSX-CTR processing. The MATXS formatted library is a 217-group VITAMIN-J structure (175 neutron groups and 42 gamma groups) based on the european data files EFF.1 and JEF.1. The TRANSX code has been

used to extract a problem dependent data library. 175-group self shielded neutron cross sections were derived corresponding to the actual background cross-sections and temperature in the stainless steel block. P5 moments and P3 moments with Bell-Hansen-Sendmaier (BHS) correction, to account for higher order anisotropy, have been generated. Transport tables created by the ANISN output options are automatically handled by the BISTRO code. Thus, 2D calculations of the FNG facility have been performed in a S16/P5 scheme.

In addition to forward flux calculation, BISTRO is able to produce automatically sensitivity coefficients S, using the Generalized Perturbation Theory: perturbation integrals in BISTRO are calculated by a module which makes use of the exact angular integration formula. In the same run, BISTRO enables the user to handle covariance matrices D and to perform uncertainty calculations [6]. The uncertainty on a response R is thus computed as

$$\left(\frac{\Delta R}{R}\right)^2 = < S^+ D S > \qquad (1)$$

In order to quantify the representativity of a measurement of the parameter R in an integral experiment E, BISTRO calculates the representativity factor

$$r_{RE} = \frac{< S_R^+ D S_E >}{\left[< S_R^+ D S_R > < S_E^+ D S_E >\right]^{\frac{1}{2}}} \qquad (2)$$

The dispersion ΔR_1^2 in the calculation of R is reduced if the experiment is performed in such a way that r_{RE} is close to unity

$$\Delta R_1^2 = \Delta R_0^2 \left(1 - r_{RE}^2\right) \qquad (3)$$

where

$$\Delta R_0^2 = < S_R^+ D S_R > \qquad (4)$$

This method has been used in the optimization of the FNG Stainless steel experiment; for example, calculations pointed out that ^{237}Np fission chamber measurements at 50 cm of depth is representative by r_{RE}=80% of the Cu DPA response in the NET TF coils.

5. Discussion and C/E comparison

The ratio of the calculated over the measured reaction rates are given in Fig.2 both for MCNP and for BISTRO calculations. The total errors on the C/E values are generally smaller than ±7%, except for $^{55}Mn(n,\gamma)$ at every position (±11%), for $^{27}Al(n,\alpha)$ at 56 cm (±11%) and $^{56}Fe(n,p)$ at 61 cm (±17%). The analysis of MCNP shows that the C/E values are close to unity and do not reveal any trend with increasing depth for detectors sensible to fast neutrons, i.e. $^{27}Al(n,\alpha)$ and $^{56}Fe(n,p)$, and for detectors sensible to slowed down neutrons, i.e. $^{55}Mn(n,\gamma)$, $^{197}Au(n,\gamma)$ and $^{235}U(n,f)$. On the contrary, for the detectors sensible to neutrons in the range 0.2 <E<14 MeV, the initial agreement between calculation and exepriment is lost for large penetration depths inside the block. This could be attributed to an inadequate treatment of Fe cross section in the region of non resolved resonances or to the Fe inelastic cross section. These results however, will be analyzed by means of a sensitivity analysis.

BISTRO results are consistent with the MCNP analysis. Nevertheless, underestimation of the flux is found for fast flux in the first 10 cm of depth. This discrepancy is probabily due to the "ray-effect" in the S_n method. BISTRO C/E values for $^{55}Mn(n,\gamma)$ and $^{197}Au(n,\gamma)$ are not shown. In fact, since

in MCNP calculations reaction rates are calculated by using both transport and dosimetric pointwise cross sections, a deeper analysis of the resonant detectors in the BISTRO procedure is required for a consistent comparison.

All the gamma heating measurements are shown in Fig.3. The corresponding BISTRO calculation is also shown for comparison, showing a satisfactory agreement. However, conclusions on these gamma measurements will be drawn after a second experimental campaign, which is planned to improve the experimental accuracy within ±10%.

5. Summary

The results of the first measurement campaign of bulk shield benchmark experiments on stainless steel have been presented. A good agreement between experiment and calculation was observed. This preliminary FNG experiment analysis confirms the validity of the European EFF.1 Library for shielding design calculations, also for damage and nuclear heating in the NET superconductive TF coils. More experimental work is in progress with new measurements of neutron and gamma spectra inside the block. The numerical analysis will be extended to the new version of the European Fusion File EFF.2. From the C/E analysis and from BISTRO sensitivity profile, a trend search method is currently implemented to improve Fe, Ni and Cr nuclear data.

Aknowledgements

This research is financed by NET under NET Subtask NDB2.1

References

[1] M. Angelone, M. Martone, M. Pillon, "The 14 MeV Frascati Neutron Generator FNG", this Conference

[2] M. Pillon, A. Santamarina, "A plan of fusion neutron benchmark experiments using the Frascati Neutron Generator (FNG)", Fusion Engrg. Des., 18 (1991) 293-296

[3] J. H. Baard, W. I. Zijp, H. J. Nolthenius, "Nuclear Data Guide for Reactor Neutron Methodology", Kluwer Academic Publisher, The Netherlands, 1989, also ECN Report ECN-89-027 (1989)

[4] G. Palmiotti, M. Salvatores, "Optimized two dimensional S_n transport (BISTRO)", Nucl. Sci. Engineering,104 (1990) 23-33

[5] P. Vontobel, "Generation of MATXS Nuclear Data Libraries", NEA Data Bank Report 1205, Paris (France), March 23, 1988.

[6] T. Parish, A. Santamarina, "Sensitivity and uncertainty analysis of the NET magnet neutronic design parameters to uncertainties in cross section data", presented at NEA-NDC Meeting, Karlsruhe (Germany), October 22,1991

Table I - Selected Dosimetry Reactions

Reaction	Half-life	90% response range (MeV)
$^{27}Al(n,\alpha)\ ^{24}Na$	15.02 h	10-14
$^{56}Fe(n,p)\ ^{56}Mn$	2.579 h	10-14
$^{115}In(n,n')\ ^{115m}In$	4.486 h	0.8-14
$^{55}Mn(n,\gamma)\ ^{56}Mn$	2.579 h	0.00017-0.06
$^{197}Au(n,\gamma)\ ^{198}Au$	2.694 d	0.00015-0.3

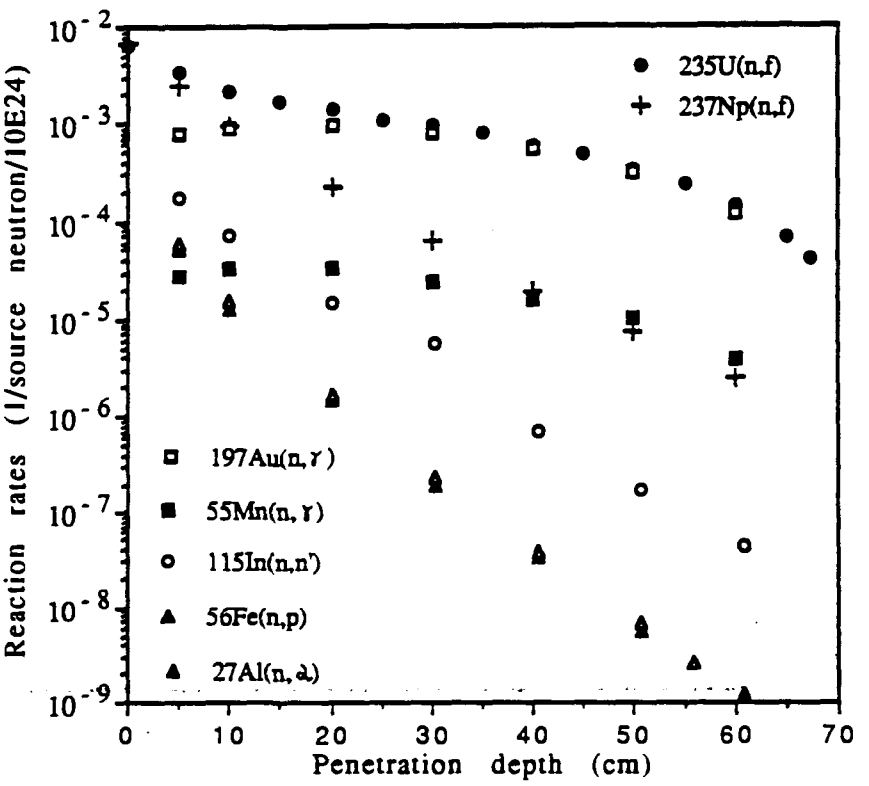

Fig. 1 - Measured reaction rates in units of reactions per 10^{24} nuclei and normalized to the totale neutron yield Y_n

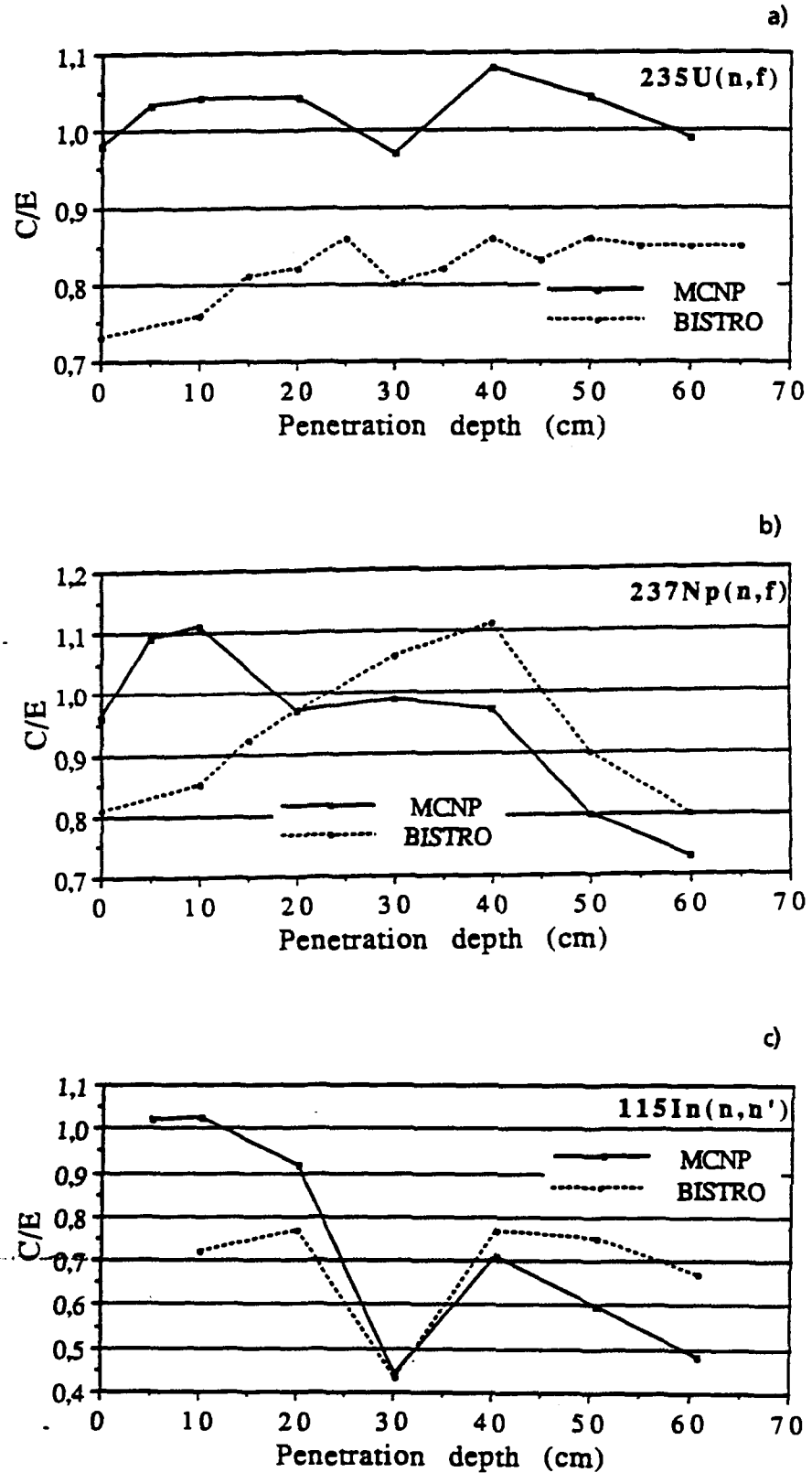

Fig. 2 - C/E ratios of calculated over experimental reaction rates

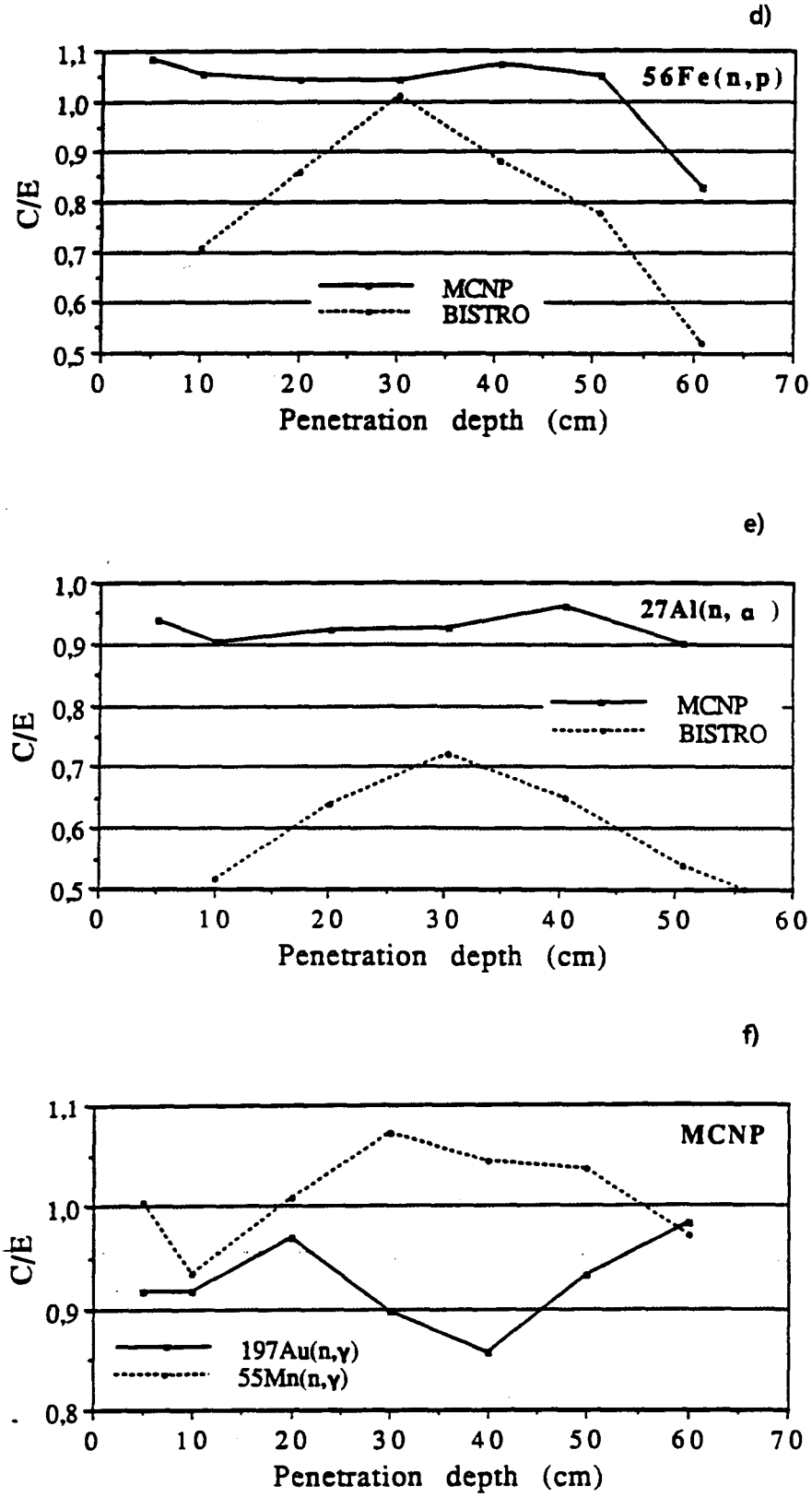

Fig. 2 - C/E ratios of calculated over experimental reaction rates

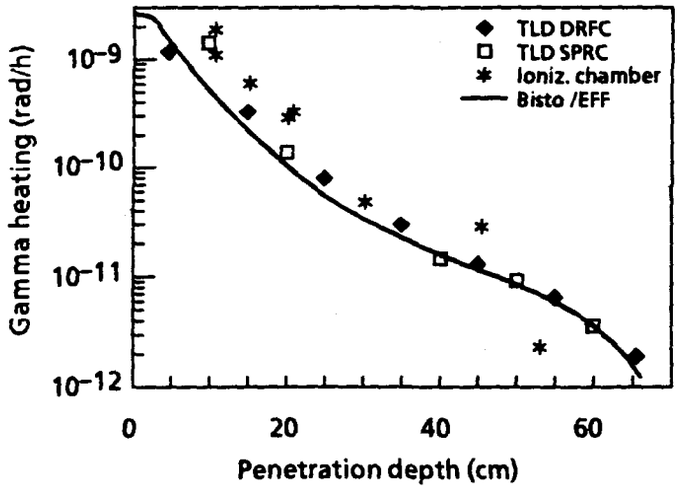

Fig. 3 - Measured gamma heating with the various techniques used, normalized to the *total neutron yield* Y_n. The solid line represents *the Bistro* calculation analysis.